Mercury Binding to the Chelation Therapy Agents DMSA and DMPS, and the Rational Design of Custom Chelators for Mercury.

Graham N. George,[*,†] *Roger C. Prince,*[‡] *Jürgen Gailer,*[§] *Gavin A. Buttigieg,*[¶] *M. Bonner Denton,*[¶] *Hugh H. Harris*[⊥] *and Ingrid J. Pickering*[†]

Department of Geological Sciences, University of Saskatchewan, Saskatoon, Saskatchewan S7N 5E2, Canada, ExxonMobil Research and Engineering Company, Annandale, New Jersey 08801, Boehringer Ingelheim Austria GmbH, Dr. Boehringer Gasse 5-11, 1120 Vienna, Austria, Department of Chemistry, The University of Arizona, Tucson, Arizona 85721, School of Chemistry, University of Sydney, Sydney, NSW 2006, Australia.

AUTHOR EMAIL ADDRESS: g.george@usask.ca

RECEIVED DATE (to be automatically inserted after your manuscript is accepted if required according to the journal that you are submitting your paper to)

TITLE RUNNING HEAD: Mercury Binding to DMSA and DMPS

---

[*] To whom correspondence should be addressed at Department of Geological Sciences, University of Saskatchewan, 114 Science Place, Saskatoon, SK, S7N 5E2, Canada. Phone: 306-966-5722, Fax: 306-966-8593, E-mail: g.george@usask.ca

[†] University of Saskatchewan
[‡] ExxonMobil Research and Engineering
[§] Boehringer Ingelheim Austria
[¶] University of Arizona
[⊥] University of Sydney

ABSTRACT

Clinical chelation therapy of mercury poisoning generally uses one or both of two drugs – *meso*-dimercaptosuccinic acid (DMSA), and dimercaptopropanesulfonic acid (DMPS), commercially sold as Chemet® and Dimaval®, respectively. We have used a combination of mercury L_{III}-edge X-ray absorption spectroscopy and density functional theory calculations to investigate the chemistry of interaction of mercuric ions with each of these chelation therapy drugs. We show that neither DMSA nor DMPS forms a true chelate complex with mercuric ions, and that these drugs should be considered sub-optimal for their clinical task of binding mercuric ions. We discuss the design criteria for a mercuric-specific chelator molecule, or "custom chelator", which might form the basis for an improved clinical treatment.

Introduction

Mercury is among the most toxic heavy elements [1,2,3] and its compounds have been linked with a number of human health problems, including neurological problems [3], myocardial infarction [4] and a possible involvement in the development of some kinds of autism [5,6]. Treatment of mercury poisoning in humans generally involves the use of chelation therapy [7,8]. A chelator is a molecule which binds a metal or metalloid ion by at least two functional groups to form a stable complex known as a chelate. Chelation therapy is the clinical treatment by which heavy metals are removed from the body through binding to a chelation therapeutic drug to form a chelate which is in most cases subsequently excreted in urine. Dimercaptosuccinic acid (DMSA) and dimercaptopropanesulfonic acid (DMPS) are commercially sold as Chemet® and Dimaval®, respectively, and have both been widely used in the chelation therapy of mercury and heavy metals [7-10]. These chelation agents are vicinal dithiols related to the now outmoded British anti-Lewisite (BAL) 2,3-dimercaptopropanol (Fig. 1a), which was developed as an antidote for the arsenical war gas Lewisite (chlorovinylarsinedichloride) [11]. BAL suffers from the disadvantages of low water solubility and a noxious smell, and so it was modified to produce DMPS (Fig. 1b), which is water soluble and nearly odorless. DMSA (Fig. 1c,d) was introduced later and has similar properties (*i.e.* excellent water solubility and no odor) with lower toxicity [7-10].

Trivalent arsenicals such as Lewisite kill by interacting with essential thiols, and in particular the dithiol lipoic acid in enzymes such as pyruvate dehydrogenase [11]. DMPS and DMSA are ideally suited for chelation therapy of As^{III} due to the stability of the five membered rings formed upon chelation of arsenic [12] (Fig. 1e) and it is widely believed that they bind a broad range of heavy metals with structures analogous to that shown for arsenic in Fig. 1e (*e.g.* Fig. 1f) [7]. DMSA occurs in *rac* and *meso* diastereomers (Fig. 1c and d, respectively), which apparently differ somewhat in their interaction with mercury [13,14]. Only the *meso* form is available commercially and used clinically, therefore in

what follows DMSA is used to indicate the *meso* form, and we do not discuss the *rac* form further. We present herein a study of the solution chemistry of mercuric ions with DMSA and DMPS, employing X-ray absorption spectroscopy and density functional theory calculations. Contrary to established thinking [*e.g.* 7], we show that the two functional groups of the chelator molecule cannot bind a common atom of mercury, and that neither DMSA nor DMPS are well-optimized molecules for chelation therapy of mercury. It therefore seems very likely that there is room for significant improvement in clinical chelation therapy. Moreover, mercury in certain tissues (*e.g.* the brain) is known to be essentially impossible to remove using DMSA and DMPS [15]. We lay out the major criteria for rational design of metal-specific or "custom chelators", and suggest directions for the development of potentially more effective drugs for mercury chelation therapy.

Materials and Methods

Sample Preparation. Reagents were purchased from Sigma Aldrich, and were of the best quality available. Samples for X-ray absorption spectroscopy were prepared at 5 mM Hg (final) in 50mM HEPES buffer pH 7.0 (final), with 30% v/v glycerol glassing agent to prevent artifacts from ice crystals. To prevent formation of precipitates, the $Hg(NO_3)_2$ was dissolved in a small quantity of dilute nitric acid prior to addition of buffer. Appropriate quantities of buffered solutions of $Hg(NO_3)_2$ and DMSA and DMPS were added, incubated for 1 min. at room temperature, and then loaded into 2x3x25mm Lucite cuvettes frozen in liquid nitrogen immediately prior to data collection. Samples for chromatography were prepared in an identical manner but using 0.1 M bis-tris buffer (pH 7.0) and without the glycerol because the high viscosity of glycerol solutions caused problems with the chromatography.

X-ray Absorption Spectroscopy. Measurements were carried out at the Stanford Synchrotron Radiation Laboratory with the SPEAR storage ring containing 60-100 mA at 3.0 GeV, on beamline 7-3 operating with a wiggler field 1.8 T, and using a Si(220) double crystal monochromator. Harmonic

rejection was accomplished by detuning one monochromator crystal to 50% peak intensity. The incident X-ray intensity was monitored using a nitrogen-filled ionization chamber, and X-ray absorption was measured as the X-ray L_α fluorescence excitation spectrum using an array of thirty germanium intrinsic detectors [16]. During data collection, samples were maintained at a temperature of approximately 10 K using a liquid helium flow cryostat. For each sample between four and six 35 minute scans were accumulated, and the absorption of a standard Hg-Sn amalgam metal foil was measured simultaneously by transmittance. The energy was calibrated with reference to the lowest energy L_{III} inflection point of the metal foil which was assumed to be 12285.0 eV. The spectrum of Hg-Sn amalgam was determined to be identical with that of a micro-particulate aqueous suspension of pure metallic mercury precipitated from aqueous $HgCl_2$ by reduction with a slight excess of sodium borohydride.

The extended X-ray absorption fine structure (EXAFS) oscillations $\chi(k)$ were quantitatively analyzed by curve-fitting using the EXAFSPAK suite of computer programs [17] as described by George *et al.* [18]. Fourier transforms were phase-corrected for Hg-S backscattering. The threshold energy E_0 was assumed to be 12305.0 eV, and *ab initio* theoretical phase and amplitude functions were calculated using the program FEFF version 8.2 [19,20].

Size Exclusion Chromatography. Size exclusion chromatography in conjunction with inductively coupled plasma atomic emission sprectroscopy (ICP-AES) was carried out as previously reported [21]. A 1 x 30 cm Superdex Peptide column served as the stationary phase and was equipped with a Rheodyne Injector (50 µl-loop). All chromatography was carried out at room temperature using a mobile phase flow rate of 1 ml/min. Mercury was monitored at the 194.227 nm emission line (order 174) and sulfur at the 182.034 nm emission (order 185). The retention times of DMSA and blue dextran on the chromatographic system were 15.3 and 8.0 min., respectively, which defined the chromatographic window.

Molecular Modeling. Density Functional Theory (DFT) molecular modeling used the program

Dmol^3 Materials Studio Version 2.2 [22,23]. DFT is a rigorous yet convenient and practical method for computing structural details of metal coordination compounds, and has been extensively validated. We expect bond-length accuracies of better than 0.05 Å, and good estimates of energetic trends between postulated molecular entities. The Becke exchange [24] and Perdew correlation [25] functionals were used to calculate both the potential during the self consistent field procedure, and the energy. Double numerical basis sets included polarization functions for all atoms. Calculations were spin-unrestricted and all electron relativistic core potentials were used. No symmetry constraints were applied (unless otherwise stated) and optimized geometries used energy tolerances of 2.0×10^{-5} Hartree.

Results and Discussion

X-ray absorption spectra can be somewhat arbitrarily divided into two regions – the near-edge region, which is sensitive to electronic structure, and the extended X-ray absorption fine structure (EXAFS) oscillations, which can be used to determine details of local structure. Near-edge spectra provide a useful fingerprint of chemical type [26], but are difficult to interpret in quantitative molecular structural terms. EXAFS spectra, on the other hand are relatively straightforward to interpret, and provide accurate distances and identities of the nearby atoms. Figure 2 shows the results of titrating aqueous mercuric nitrate (approximating Hg^{2+} ions) with increasing amounts of the two chelators DMSA and DMPS. Panels A and B show the Hg L_{III} near-edge spectra of samples with increasing DMSA (A) and DMPS (B). DMSA shows essentially identical near-edge spectra with chelator:Hg levels of 1:1 and higher. In contrast, DMPS shows gradual changes until chelator:Hg levels of 4:1 are achieved, indicating fundamental differences in solution chemistry. Nevertheless, the near-edge spectra of the two 1:1 mixtures are very similar.

Panels C and D of Fig. 2 show the EXAFS Fourier transforms, phase-corrected for Hg-S backscattering, for the samples of panels A and B. All data were analyzed by quantitative curve-fitting and the numerical results are given in Table 1. Structurally characterized mercury compounds exhibit coordination numbers between two and eight [27]. Examination of the Cambridge Structural Database indicates that most sulfur-bound mercury species are either two- or four-coordinate and these show typical Hg-S bond-lengths of 2.35(1) and 2.55(3) Å, respectively. The two-coordinate species are always close to linear (S-Hg-S angle 177(4)º) while the four-coordinate species are approximately tetrahedral (S-Hg-S angle 110(2)º). For DMSA:Hg of 1:1 and higher, the EXAFS clearly shows backscattering from two sulfur atoms at 2.345(1) Å, consistent with a two coordinate species. Similar results (two Hg-S at 2.367(2) Å) are seen for DMPS:Hg of 1:1. Higher ratios (DMPS:Hg 4:1 and 9:1) give a Hg-S coordination number of 4 with an average bond-length of 2.513(2) Å, which is consistent with a four-coordinate geometry. Intermediate ratios (DMPS:Hg 2:1) give mixtures of two and four

coordinate species. In agreement with this, principal component analyses of the sets of near-edge spectra shown in Fig. 2A and B indicate that these can be explained as mixtures of only two and three components for DMSA and DMPS, respectively. Since the sulfurs in a single DMSA or DMPS molecule are not sufficiently separated to accommodate a linear two-coordinate S-Hg-S species, a true 1:1 complex such as shown in Fig. 1f would be impossibly strained. We therefore conclude that more complex structures must be occurring with at least two DMSA or DMPS molecules and at least two mercury atoms.

Size exclusion chromatography of the DMSA complexes (Fig. 3) shows common column retention times of 13 minutes for sulfur and mercury using a DMSA:Hg ratio of 1:1. This suggests a single molecular entity, rather than a broad distribution of polymers, and EXAFS spectroscopy of a purified sample from this experiment gave identical data to that shown in Figures 2 (not illustrated). With higher levels of DMSA the primary mercury species is the same as the DMSA:Hg ratio of 1:1, and unreacted DMSA is eluted with a column retention time of 15.3 minutes. A small additional species with a column retention time of 11.8 minutes was also observed (Fig. 3). As we will discuss below, the primary 13.0 minute species is likely to be a binuclear species, formulated as $Hg_2(DMSA)_2$ and the secondary 11.8 minute species observed with higher DMSA:Hg ratios is very likely the trinuclear species $Hg_3(DMSA)_3$. The simplest candidate molecule for the primary reaction product thus involves two DMSA molecules and two mercury atoms.

Density functional structural optimizations of the two possible diastereomers of $Hg_2(DMSA)_2$ are shown in Fig. 4. For each diasteriomer, calculations were performed on the acids, anionic species and anionic species with a single water associated with each carboxylate. These showed only very subtle structural differences, and only the anionic hydrated species is shown for each diasteriomer (with water molecules omitted for clarity). The expected occurrence of two diasteriomers in solution explains the absence of a clear Hg···Hg backscattering in the EXAFS Fourier transforms of Fig. 2. The two diasteriomers have different Hg···Hg distances which results in near-cancellation of this interaction (Fig.

5A). The curve-fitting analysis shown in Fig. 5B includes all outer shell interactions (apart from hydrogens), including two different Hg···Hg distances, based on the results of density functional calculations shown in Fig. 4. The excellent match between the calculated and experimental curves adds more weight to the suggestion that the structures of Fig. 4 are present in solution. Further density functional calculations (not illustrated) indicate that the ring-shaped trinuclear $Hg_3(DMSA)_3$ is also expected to be a stable entity, with additional long (~3Å) Hg····S bonds involving adjacent DMSA sulfurs in conformers of both possible diasteriomers. As we have discussed, the observed chromatography retention times (Fig. 3) are also consistent with the primary product being the binuclear species (Fig. 4).

As we have discussed above, DMPS forms a similar species with DMPS:Hg ratios of 1:1. The number of possible diasteriomers (four conformers) is greater with DMPS than with DMSA because the carbon atom bearing the $-CH_2SO_3^-$ moiety (Fig. 1) is chiral, and commercially available DMPS is a racemic mixture of L- and D- forms. Figure 6 a and b show computed structures for two possible diasteriomers; the other forms are similar with slightly differing Hg···Hg distances, as with DMSA. At higher DMPS:Hg ratios (*e.g.* 4:1), four-coordinate species are observed to form (Fig. 6d). Density functional calculations indicate that true double-chelate complexes, in which both thiolates of each of two DMPS molecules are bound to the metal (Fig. 6c), ought to be stable. Indeed, a number of low-molecular weight dithiolane double-chelates have been characterized [28]. However, the fact that exclusively four-coordinate species do not form at DMPS:Hg ratios lower than 4:1 indicates that significant quantities of true chelate complexes are not formed in our experiments. In agreement with this, chromatography of a sample with Hg and excess DMPS (not illustrated) gives DMPS:Hg ratios of 4:1 for the co-eluting sulfur and mercury peaks, suggesting structures related to the computed 4:1 species of Figure 6d.

We now address the question of why DMSA does not form a four-coordinate species as observed for DMPS. The most likely reason for this is that at the physiological pH used, the molecule

would bear too large a negative charge to be stable. For example, a four-coordinate double chelate (one Hg, two DMSA) analogous to figure 6c, would bear a charge of 6-, while the species with four DMSA molecules coordinating a single mercuric ion (as monofunctional reagents) analogous to figure 6d, would bear a massive negative charge of 14-. Furthermore, the negatively charged carboxylate groups are much closer to the coordinating thiolate group than is the sulfonate of DMPS, and this proximity would further destabilize the complex. In agreement with this, DFT calculations predict stability of uncharged (protonated), but not of the charged species; in the charged case the ligands to the metal dissociate during the geometry optimization. DMPS, on the other hand, which bears only a single negative charge, can form stable four-coordinate species, and this is evident both from the experimental data (Fig. 2), and from the calculations (Fig. 6).

One criterion for an effective drug for chelation therapy is that the chelator should interact in a stoichiometric manner with its target metal. In other words, if the chelation drug is exposed to the target metal ion *in vivo* then it should be able to bind effectively all by itself, without the need for an additional molecular entity. We have shown that this criterion is not fulfilled by the clinically used mercury chelation therapeutic drugs, DMSA and DMPS (Chemet® and Dimaval®). There is no doubt that DMSA and DMPS are effective, to some degree, in the clinical treatment of mercury poisoning [7-10,29,30], although not in all cases [31]. Nevertheless, we have presented strong evidence that these compounds are likely sub-optimal for clinical chelation therapy by a considerable margin, and we expect that considerable improvements should be possible. We now consider the criteria for the rational design of a more effective agent for mercury chelation therapy. Quantum chemical methods can provide criteria for the design of a drug that will not only bind mercuric ions with considerable tenacity but also with a high degree of specificity for mercuric ions above other cations – in effect a "custom chelator".

As we have discussed above, one of the preferred coordinations of mercuric ions is a linear, two-coordinate geometry. A custom chelator optimized for such digonal coordination should present the metal with two thiol groups whose sulfurs are separated by twice the optimal Hg-S distance (*i.e.*

2×2.345Å). We have used methyl mercury mercaptide ($CH_3SHgSCH_3$) as a minimal model to define the optimum binding geometry of Hg^{2+} to alkyl thiolate donors. Figure 7 shows the calculated energy of this molecule as a function of Hg-S bond-length, and of C-S-Hg and S-Hg-S bond-angles. Our density functional theory calculations underestimate bond-lengths by about 0.05Å (relative to test molecules of accurately known structure [27]), and slightly better absolute values for an ideal bond-length can be derived from examination of the Cambridge Structural Database [27]. Figure 7A shows a sharp minimum with an optimum bond-length 2.30 Å, indicating that precise control of this parameter is required in a custom chelator, and the same is true of the C-S-Hg bond-angle shown in Fig. 7B, with an optimum of about 103°. In contrast, the S-Hg-S bond-angle is rather less sensitive, and can deviate by nearly 10° about the optimum of 180° with little energetic penalty. The energetic dependence of the C-SHgS-C torsion angle is shown in Fig. 8, with a clear minimum at 90°. Less rigorous molecular modeling methods, such as molecular mechanics (MM2 or MM3) or semi-empirical methods such as MOPAC (PM3 or PM5 Hamiltonians) or MNDOd, predict structures with this angle closer to the more intuitive value of 180° with the methyl groups as far away from each other as possible. This illustrates the advantages of the more rigorous density functional method. Examination of the computed molecular orbitals shows that the highest occupied molecular orbital is made up of orthogonal S 3p and Hg 5d contributions (Fig. 8), explaining the 90° torsion angle. Examination of linear S-Hg-S species in the Cambridge Structure Database [27] substantiates our conclusion of an approximately 90° torsion angle. In cases where the ~90° torsion angle is not observed there are intermolecular bonding or other interactions within the extended solid that can explain this deviation.

The structure required for the immediate ligands to mercury in a custom chelator is thus well defined. The next step is to design an organic molecule that can hold the thiol donors in the correct orientation and proximity. We have adopted a hybrid approach in which the sulfurs and adjacent carbon atoms were held rigid at their optimal positions and an organic framework was then refined using semi-empirical methods, (MOPAC 2002, employing a PM3 Hamiltonian) which have the advantage of better

speed. The structure was adjusted by judicious addition of framework atoms such as carbon until it appeared strain free. The total structure was then refined, without restraints, using the density functional method and the Hg-S bond-lengths and angles examined for signs of distortions. The calculated energy difference between the ligand and the metal-bound form was also examined as a crude index of stability. A large number of possible structures were generated using this approach and the one shown in Figure 9 should be considered as only one possible candidate. Additional functional groups can be added to adjust the compound's water solubility (*e.g.* carboxylates, sulfonates etc.) and membrane crossing properties, although care must be taken not to interfere with the mercury binding parts of the molecule. We note that there are many additional factors in the design of an effective drug that we have not considered here, such as inherent toxicity of the custom chelator itself, and how readily the chelate (once formed) is excreted. As far as metal specificity is concerned, this will be primarily conferred from the coordination geometry and bond-length. For example, numerous zinc thiolate species have been characterized, with a bond-length of about 2.35 Å (*i.e.* about the same as the two-coordinate Hg-S bond-length) [27], but with a tetrahedral coordination geometry. On the other hand cuprous ions readily adopt a digonal coordination geometry, but the Cu-S bond-length of around 2.15Å [27] means that the mercury custom chelator is too big to accommodate cuprous ions.

In summary, we have used X-ray absorption spectroscopy to show that the two clinically used mercury chelation therapeutic drugs, DMSA and DMPS (Chemet® and Dimaval®) cannot work as true chelators and are thus sub-optimal for their clinical role by a considerable margin. We have also outlined the chemical factors that will be important in the design of a chelation therapeutic drug with specificity for mercuric ions, a custom chelator. Our approach could also be used to design therapeutic chelators for other elements, and of course similar approaches could be used to design insoluble chelators to remove mercury and other elements from water and waste streams.

Acknowledgements This work was carried out at the Stanford Synchrotron Radiation Laboratory which is funded by the DOE, OBES and OBER, and the NIH, NCRR BMTP. GNG and IJP were supported in part by Canada Research Chair awards, the University of Saskatchewan, and the Province of Saskatchewan.

Figure Captions

Figure 1. Structures of (a) British anti-lewisite (BAL), (b) dimercaptopropanesulfonic acid (DMPS), (c) *meso*-dimercaptosuccinic acid (*meso*-DMSA), (d) *rac*-DMSA, (e) As^{3+} chelate with BAL and (f) structure previously proposed for DMSA chelate with Hg^{2+}.

Figure 2. X-ray Absorption Spectroscopy titration of Hg^{2+} with DMSA and with DMPS. A and B show the Hg L_{III} near-edge spectra, while C and D show the EXAFS Fourier transforms (phase-corrected for Hg-S backscattering). The ratios of DMSA:Hg^{2+} and DMPS:Hg^{2+} are indicated on the figure. The vertical broken lines in D show the expected peak-positions for two- (lower) and for four-coordinate mercury.

Figure 3. Size exclusion / ICP-AES chromatography of different DMSA:Hg^{2+} ratios. The DMSA:Hg^{2+} ratios are shown in the figure. The radii of spheres of equivalent volume to the computed electron density for the trinuclear $Hg_3(DMSA)_3$ and binuclear $Hg_2(DMSA)_2$ species, and for free DMSA were approximately linearly related to the retention times (not illustrated) confirming the peak assignments to trinuclear and binuclear species.

Figure 4. Calculated structures of the two diasteriomers of the smallest possible DMSA:Hg^{2+} complex. Carbon atoms are depicted as being dark gray, oxygen as red, hydrogen as white, mercury as light gray and sulfur as yellow.

Figure 5. A: The effects of dissimilar Hg···Hg distances computed for the two diasteriomers, showing

both the Fourier transform and EXAFS oscillations (insets); *(a)* shows the expected EXAFS Fourier transform from one diasteriomer including Hg-S and Hg····Hg interactions (the inset shows Hg····Hg EXAFS) and *(b)* shows the Fourier transform using the two different Hg····Hg interatomic distances computed for the two diasteriomers (the inset shows how the two Hg····Hg EXAFS components cancel, and is identically scaled to the inset in *(a)*). B: EXAFS curve-fitting analysis of data of Figure 2 (DMSA:Hg^{2+} ratio of 1:1), showing Fourier transforms and total EXAFS oscillations (inset). The solid lines show the experimental data and the broken lines show the computed curve using the best-fit Hg-S and the outer shell Hg····Hg and Hg····C distances computed using DFT.

Figure 6. Calculated structures of possible Hg^{2+} – DMPS complexes. (a) and (b) show two of the four possible diasteriomers for linear Hg coordination, (c) shows the true double chelate, and (d) shows the 4:1 complex detected by chromatography. The color scheme for atoms is the same as that used in Fig. 4.

Figure 7. Calculated energy profile for Hg-S bond-length, C-S-Hg bond-angle and S-Hg-S bond-angle for *bis*-methylmercaptan-mercury(II). The binding energy of the ordinates is defined as the energy required to separate all atoms to infinity.

Figure 8. Calculated energy profile for the C-S-(Hg)-S-C torsion angle, showing the 90° minimum and the 0.03 $Å^2$ isosurface of the highest occupied molecular orbital.

Figure 9. Structure of a possible custom chelator for Hg^{2+} based on digonal thiolate coordination (see text for details). Nitrogen atoms are shown in blue, otherwise the color scheme is as for figure 4. This chelator (2-[4-(2-Mercapto-ethylamino)-phenyl amino]-ethanethiol) is merely an example of the type of molecule which might be used, and is not a serious candidate for a custom chelator. More optimal structures might incorporate thiols rigidly held in their ideal positions.

Table 1. EXAFS curve-fitting results for titrations of Hg^{2+} with DMSA and DMPS[a]

Drug	*n*	*Atom*	*N*	*R*	σ^2	ΔE_0	*F*
–	0[b]	O	2	2.162(11)	0.0082(6)	-15.3(20)	0.504
DMSA	0.5	S	1	2.391(2)	0.0032(2)	-18.5(8)	0.384
		O	1	2.123(15)	0.0066(3)		
	1.0	S	2	2.344(2)	0.0028(1)	-18.0(6)	0.318[c]
	2.0	S	2	2.346(2)	0.0025(1)	-17.5(6)	0.283
	4.0	S	2	2.344(2)	0.0027(1)	-17.6(6)	0.259
DMPS	0.5	S	1	2.384(2)	0.0039(1)	-18.3(8)	0.513
		O	1	2.127(15)	0.0089(4)		
	1.0	S	2	2.367(2)	0.0047(1)	-18.4(4)	0.242
	2.0	S	1.3(1)	2.397(5)	0.0047	-18.3(4)	0.439[d]
		S	1.7(1)	2.528(6)	0.0059		
	4.0	S	4	2.514(2)	0.0066(1)	-17.8(5)	0.293
	9.0	S	4	2.514(2)	0.0059(1)	-18.2(5)	0.244

a. *n* is the mole-ratio of drug (DMSA or DMPS) to Hg^{2+}. Coordination numbers *N*, interatomic distances *R* are given in Å, Debye-Waller factors σ^2 (the mean-square deviations in interatomic distance) in $Å^2$, and the threshold energy shifts ΔE_0 are given in eV. The values in parentheses are the estimated standard deviations obtained from the diagonal elements of the covariance matrix. The fit-error function *F* is defined as $[\Sigma k^6(\chi_{calc.}-\chi_{expt})^2/\Sigma\chi_{expt}^2]^{½}$.

b. The presence of additional longer-range Hg-O interactions is also indicated by the fits, specifically 2 Hg-O at 2.57(2) Å, ~1 Hg-O at 2.74(2) Å, ~1 Hg-O at 3.04(1) Å and ~1 Hg-O at 3.31(2) Å. The bond-length for a purely digonal Hg-O coordination is 2.08 Å, and the 0.08 Å longer Hg-O bond-length is consistent with longer-distance oxygen ligation, which are common

in mercury complexes [27].

c. The somewhat higher fit-error in this case is mainly due to slightly higher noise content in the spectrum.

d. The fit was achieved by fixing σ^2 at values obtained for the two-coordinate and four-coordinate species (n of 1 and 4, respectively) and refining the apparent coordination numbers N. This is necessary due to the high correlation between σ^2 and N in the refinement. The larger fit-error reflects the poorer fit that was obtained with this method.

Table 2. Selected bond-lengths (Å) and angles (º) computed for DMSA Hg^{2+} complexes.

	Diasteriomer 1	Diasteriomer 2
Hg-S	2.33, 2.38 2.38, 2.34	2.32, 2.31 2.33, 2.33
Hg···Hg	3.04	3.13
C-S-Hg	100.5, 113.5 113.5, 100.5	106.5, 110.7 113.9, 106.4
S-Hg-S	175.2, 174.4	168.2, 163.6

References

(1). Clarkson, T. W. (1998) Human Toxicology of Mercury. *J. Tr. Elem. Exp. Med.* **11**, 303-317.

(2). Clarkson, T. W. (2002) The Three Modern Faces of Mercury. *Env. Health Persp.* **110** (suppl. 1), 11-23.

(3). Weiss, B., Clarkson, T. W., and Simon, W. (2002) Silent Latency Periods in Methylmercury Poisoning and in Neurodegenerative Disease. *Env. Health Persp.* **110** (suppl. 5), 851-854.

(4). Guallar, M. D., Sanz-Gallardo, M. I., van't Veer, P., Bode, P., Aro, A., Gómez-Aracena, J., Kark, J. D., Riemersma, R. A., Martín-Moreno, J. M., and Kok, F. J. (2002) Mercury, Fish Oils, and the risk of Myocardial Infarction. *N. Engl. J. Med.* **347**, 1747-1754.

(5). Bernard, S., Enayati, A., Redwood, L., Roger, H., and Binstock, T. (2001) Autism: A Novel Form of Mercury Poisoning. *Med. Hypot.* **56**, 462-471.

(6). Bernard, S., Enayati, A., Roger, H., Binstock, T., and Redwood, L. (2002) The Role of Mercury in the Pathogenesis of Autism. *Mol. Psych.* **7**, S42-S43.

(7). Aposhian, H. V., Maiorino, R. M., Gonzalez-Ramirez, D., Zuniga-Charles, M., Xu, Z., Hurlbut, K. M., Junco-Munoz, P., Dart, R. C., and Aposhian, M. M. (1995) Mobilization of Heavy Metals by Newer, Therapeutically Useful Chelating agents. *Toxicology* **97**, 23-38.

(8). Campbell, J. R., Clarkson, T. W. and Omar, M. D. (1986) The therapeutic use of 2,3-dimercaptopropane-1-sulfonate in two cases of inorganic mercury poisoning. *J. Am. Med. Assoc.* **256**, 3127-3130.

(9). Gonzalez-Ramizez, D., Maiorino, R. M., Zuniga-Charles, M., Xu, Z., Hurlbut, K. M., Junco-Munoz, P., Aposhian, M. M., Dart, R. C., Diaz Gama, J. H., Echeverra, D., Woods, J. S. and

Aposhian, H. V. (1995) Sodium 2,3-Dimercaptopropane-1-Sulfonate Challenge Test for Mercury in Humans: II. Urinary Mercury, Porphyrins and Neurobehavioral Changes of Dental Workers in Monterrey, Mexico. *J. Pharmacol. Exp. Ther.* **272**, 264-274

(10). Maiorino, R. M., Aposhian, M. M., Xu, Z.-F., Li, Y., Polt, R. L., and Aposhian, H. V. (1993) Determination and Metabolism of Dithiol Chelating Agents. XV. the *Meso*-2,3-Dimercaptosuccinic Acid-Cysteine (1:2) Mixed Dilsulfide, a Major Urinary Metabolite of DMSA in the Human, Increases the Urinary Excretion of Lead in the rat. *J. Pharmacol. Exp. Ther.* **267**, 1221-1226.

(11). Ord, M. G., and Stocken, L. A. (2000) A Contribution to Chemical Defense in World War II. *Trends in Biochem. Sci.* **25**, 253-256.

(12). von Döllen, A., and Strasdeit, H. (1998) Models for the Inhibition of Dithiol-containing Enzymes by organoarsenic compounds: Synthetic Routes and the structure of [PhAs(HlipS_2)] (HlipS_2^{2-} = reduced Lipoic Acid). *Eur. J. Inorg. Chem.* 61-66.

(13). Fang, X., and Fernando, Q. (1994) Synthesis, Structure and Properties of *rac*-2,3-Dimercaptosuccinic Acid, a Potentially Useful Chelating Agent for Toxic Metals. *Chem. Res. Toxicol.* **7**, 148-156.

(14). Fang, X., Hua, F., and Fernando, Q. (1996) Comparison of *rac*- and *meso*-2,3-Dimercaptosuccinic Acids for Chelation of Mercury and Cadmium Using Chemical Speciation Models. *Chem. Res. Toxicol.* **9**, 284-290.

(15). Clarkson, T. W., Magos, L., and Myers, G. J. (2003) The Toxicology of Mercury – Current Exposures and Clinical Manifestations. *N. Engl. J. Med.* **349**, 1731-1737.

(16). Cramer, S. P., Tench, O., Yocum, M., and George, G. N. (1988) A 13-Element Ge Detector for Fluorescence EXAFS. *Nucl. Instrum. Meth.* **A266**, 586-591.

(17). http://ssrl.slac.stanford.edu/exafspak.html

(18). George, G. N., Hilton, J. Temple, C., Prince, R. C., and Rajagopalan, K. V. (1999) The Structure of the Molybdenum Site of Dimethylsulfoxide Reductase. *J. Am. Chem. Soc.* **121**, 1256-1266.

(19). Rehr, J. J., Mustre de Leon, J., Zabinsky, S. I., and Albers, R. C. (1991) Theoretical x-ray absorption fine structure standards. *J. Am. Chem. Soc.* **113**, 5135-5140.

(20). Mustre de Leon, J., Rehr, J. J., Zabinsky, S. I., and Albers, R. C. (1991) Ab initio curved-wave x-ray-absorption fine structure. *Phys. Rev.* **44**, 4146-4156.

(21). Gailer, J., George, G. N., Harris, H. H., Pickering, I. J., Prince, R. C., Buttigieg, G. A., Glass, R. S., and Denton, M. B. (2002) Synthesis, purification and structural characterization of the dimethyldiselenoarsinate anion. *Inorg. Chem.* **41**, 5427-5432.

(22). Delley, B. (1990) An all-electron numerical method for solving the local density functional for polyatomic molecules. *J. Chem. Phys.* **92**, 508-517.

(23). Delley, B. (2000) From molecules to solids with the DMol3 approach *J. Chem. Phys*. **113**, 7756-7764.

(24). Becke, A. D. (1988) A multicenter numerical integration scheme for polyatomic molecules. *J. Chem. Phys*. **88**, 2547-2553.

(25). Perdew, J. P., and Wang, Y. (1992) Accurate and simple analytic representation of the electron-gas correlation energy. *Phys. Rev. B* **45**, 13244-13249.

(26). Harris, H. H., Pickering, I. J., and George, G. N. (2003) The Chemical Form of Mercury in Fish. *Science*, **301**, 1203.

(27). Allen, F. H., Kennard, O., and Watson, D. G. (1994) Crystallographic databases: Search and retrieval of information from the Cambridge Structural Database. *Struct. Correl.* **1**, 71-110.

(28). Govindaswamy, N., Moy, J., Millar, M., and Koch, S. A. (1992) A Distorted $[Hg(SR)_4]^{2-}$ Complex with Alkanethiolate Ligands: The Fictile Coordination Sphere of Monomeric $[Hg(SR)_x]$ Complexes. *Inorg. Chem.* **31**, 5343-5344.

(29). Garza-Ocanas, L., Torres-Alanis, O., and Pineyro-Lopez, A. (1997) Urinary mercury in twelve cases of cutaneous mercurous chloride (calomel) exposure: effect of sodium 2,3-dimercaptopropane-1-sulfonate (DMPS) therapy. *J. Toxicol., Clin. Toxicol.* **35**, 653-655.

(30). Böse-O'Reilly, S., Drasch, S., Beinhoff, C., Maydla, S., Voskob, M. R., Roidera G., and Dzajaa, D. (2003) The Mt. Diwata study on the Philippines 2000 – treatment of mercury intoxicated inhabitants of a gold mining area with DMPS (2,3-Dimercapto-1-propane-sulfonic acid, Dimaval®). *Sci. Tot. Env.* **307**, 71-82.

(31). Pfab, R., Mueckter, H., Roider, G. and Zilker, T. (1996) Clinical course of severe poisoning with thiomersal. *J. Toxicol., Clin. Toxicol.* **34**, 453-460.

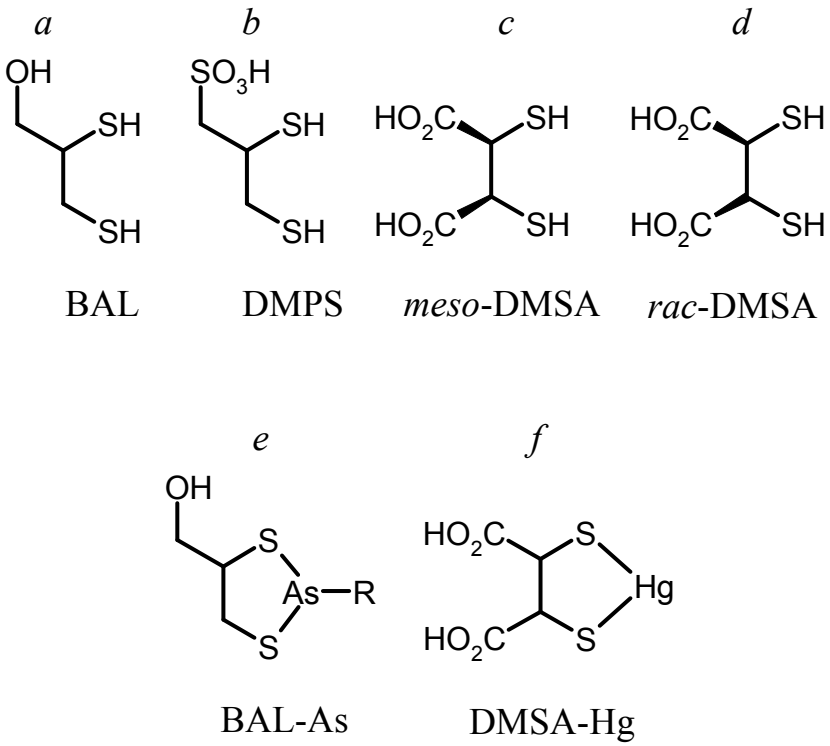
a
b
c
d
OH
SH
SH
SO3H
SH
SH
HO2C
SH
HO2C
SH
HO2C
SH
HO2C
SH
BAL
DMPS
meso-DMSA
rac-DMSA
e
f
OH
S
As
R
S
HO2C
S
Hg
HO2C
S
BAL-As
DMSA-Hg

Figure 1

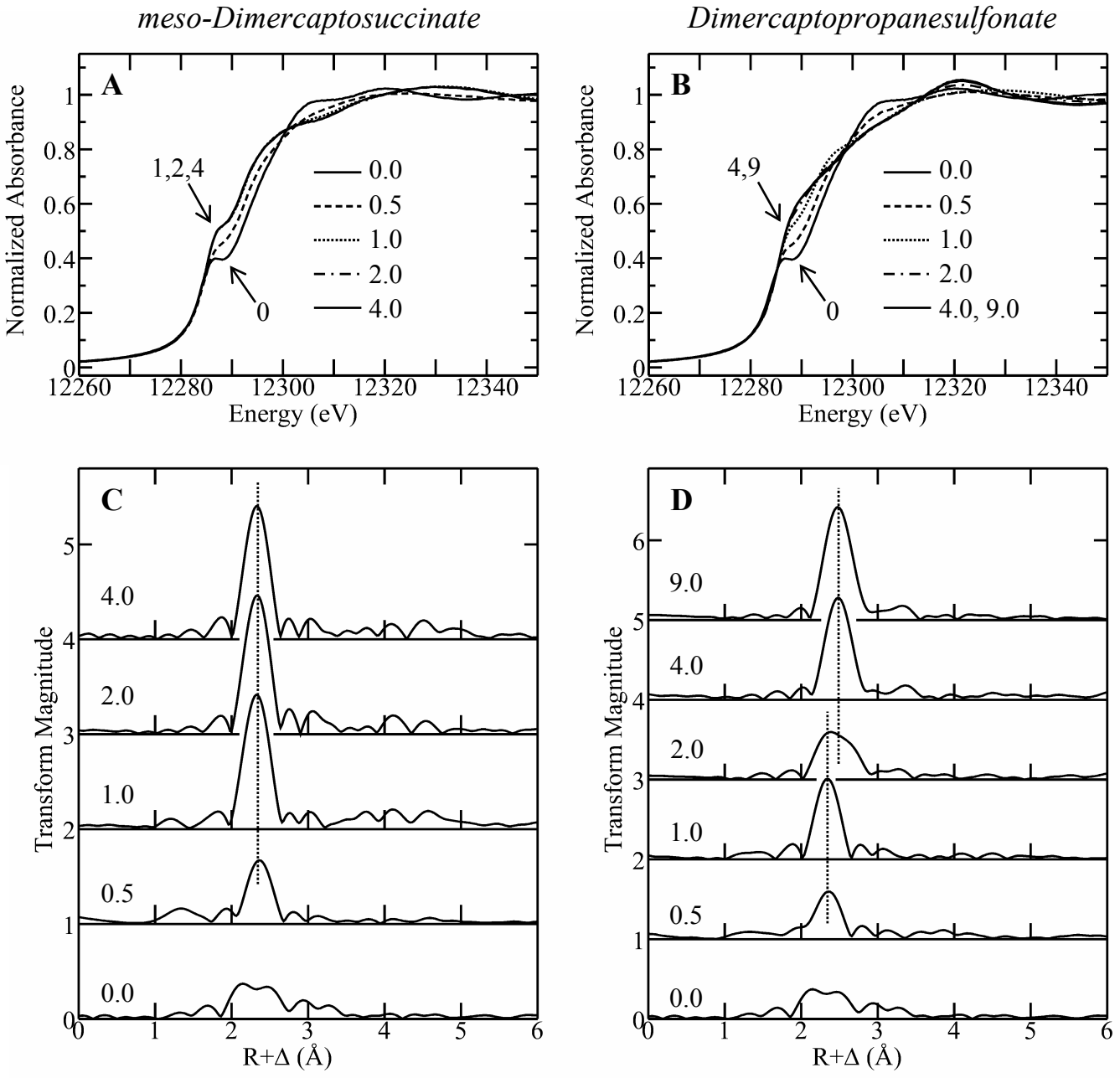
meso-Dimercaptosuccinate
Dimercaptopropanesulfonate
A
B
C
D
Normalized Absorbance
Energy (eV)
1,2,4
0
4,9
0.0
0.5
1.0
2.0
4.0
4.0, 9.0
Transform Magnitude
R+Δ (Å)
9.0

Figure 2

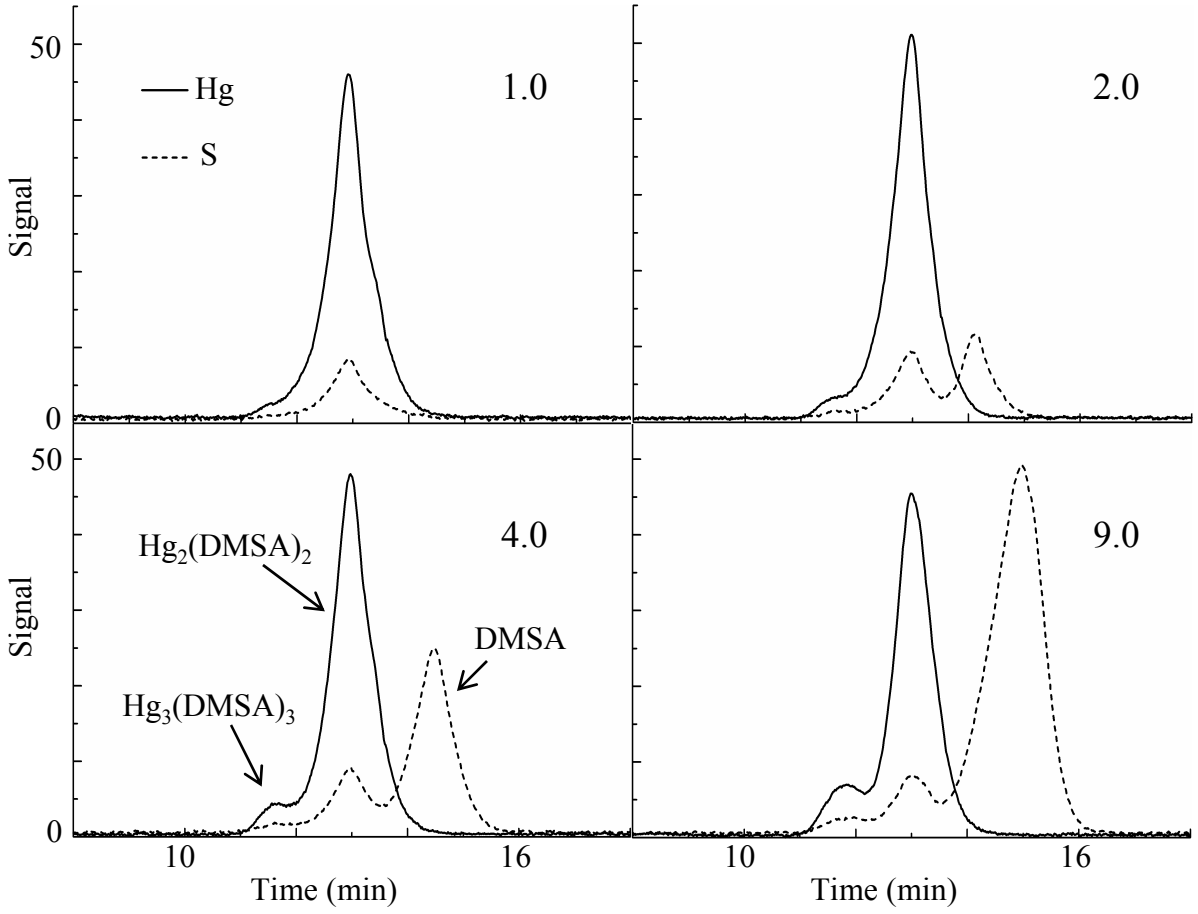
50
0
Signal
Hg
S
1.0
2.0
4.0
9.0
$Hg_2(DMSA)_2$
$Hg_3(DMSA)_3$
DMSA
10
16
Time (min)

Figure 3

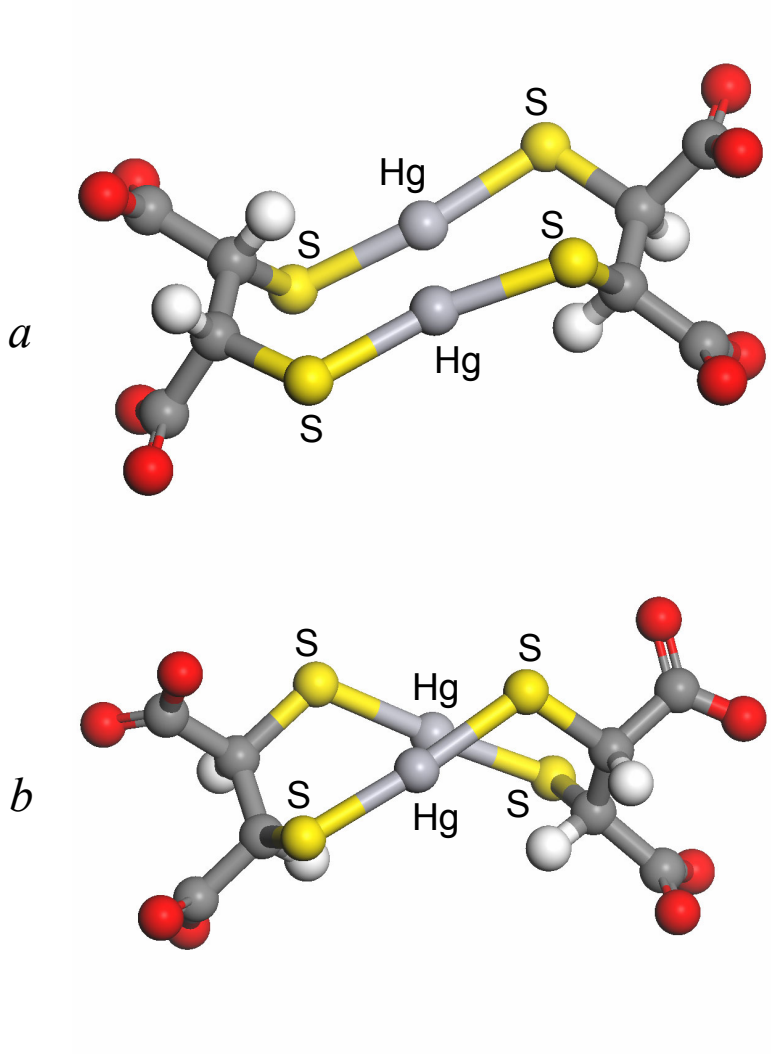

Figure 4

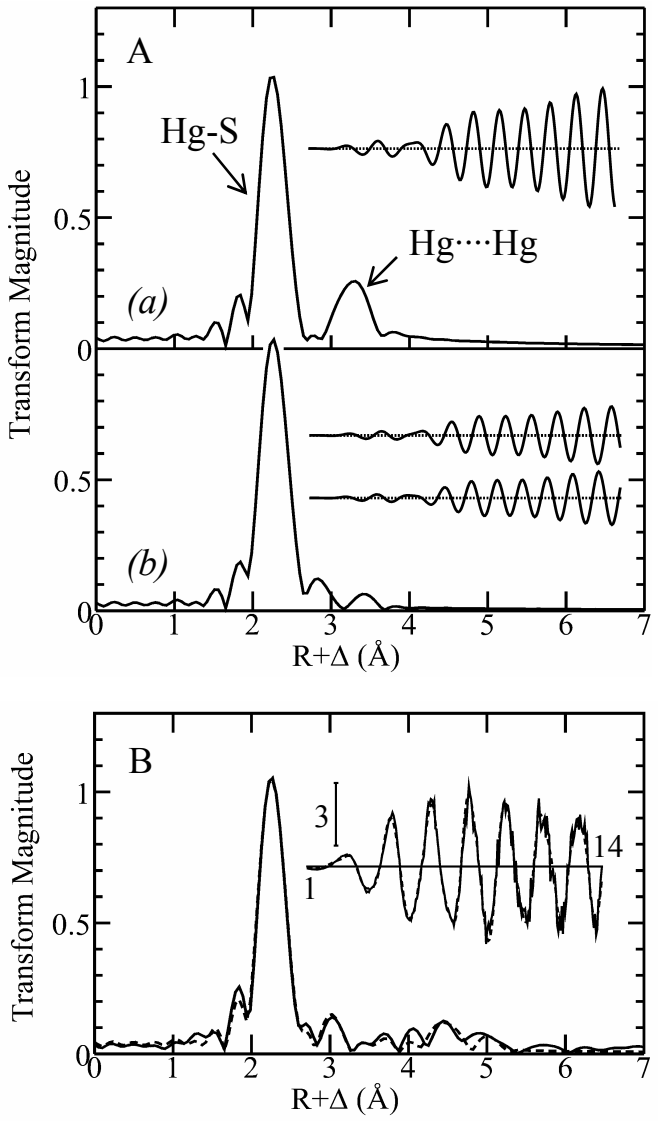

Figure 5

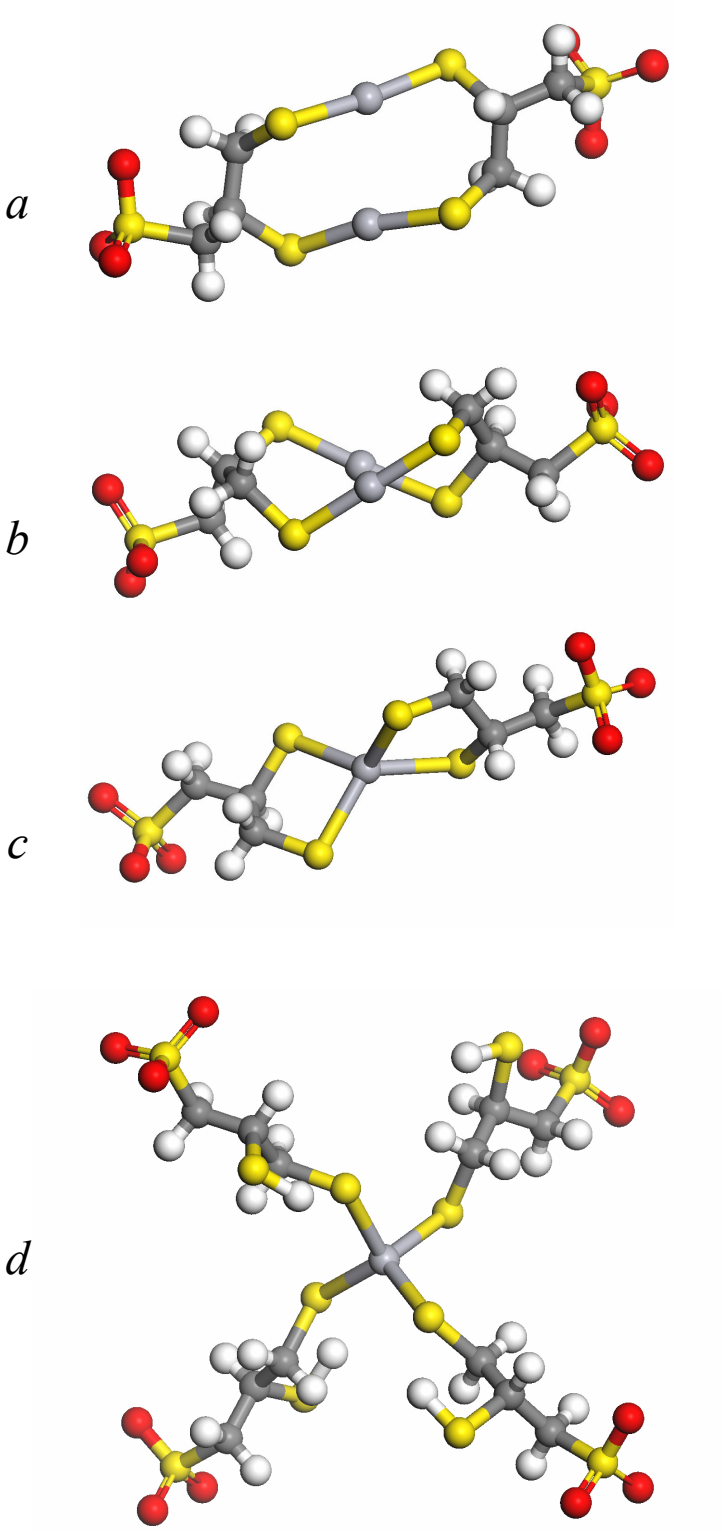

Figure 6

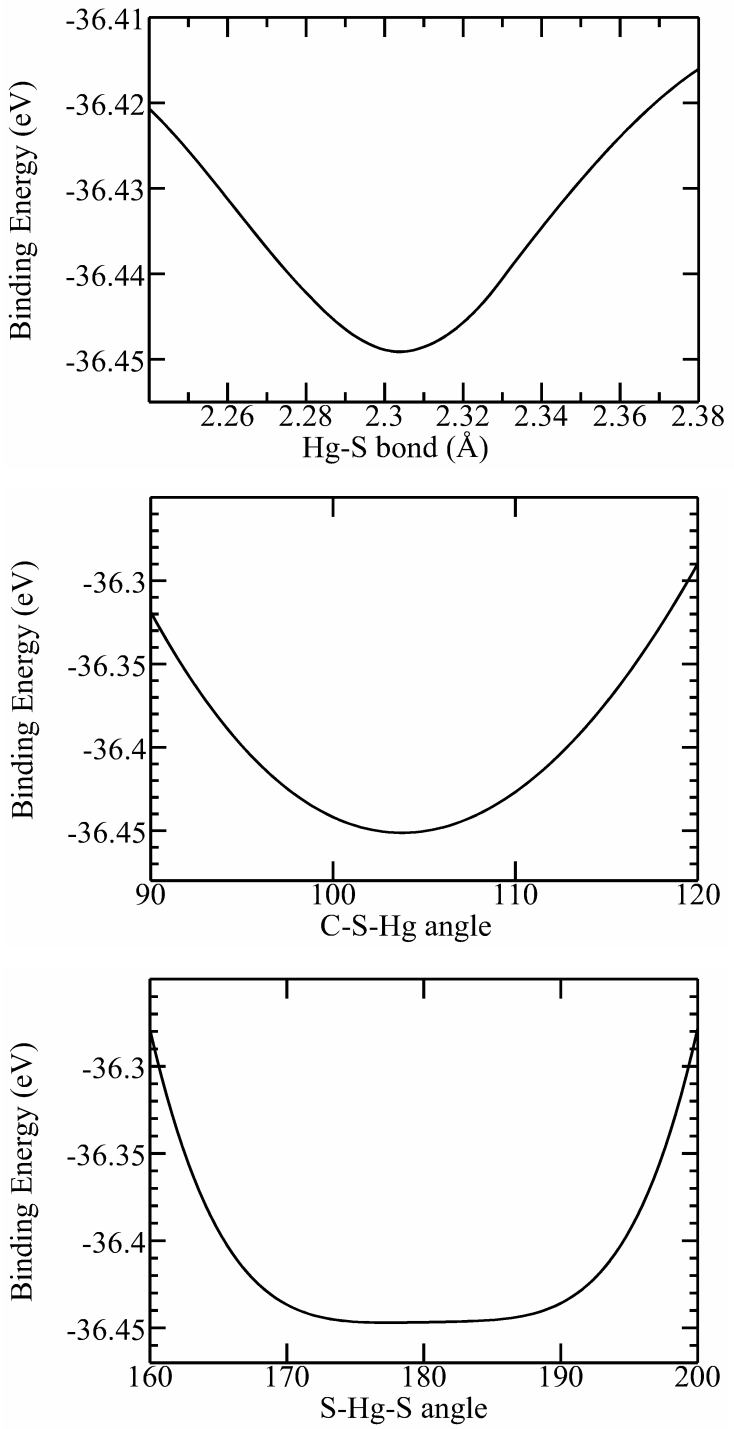
Binding Energy (eV)
-36.41
-36.42
-36.43
-36.44
-36.45
2.26
2.28
2.3
2.32
2.34
2.36
2.38
Hg-S bond (Å)
Binding Energy (eV)
-36.3
-36.35
-36.4
-36.45
90
100
110
120
C-S-Hg angle
Binding Energy (eV)
-36.3
-36.35
-36.4
-36.45
160
170
180
190
200
S-Hg-S angle

Figure 7

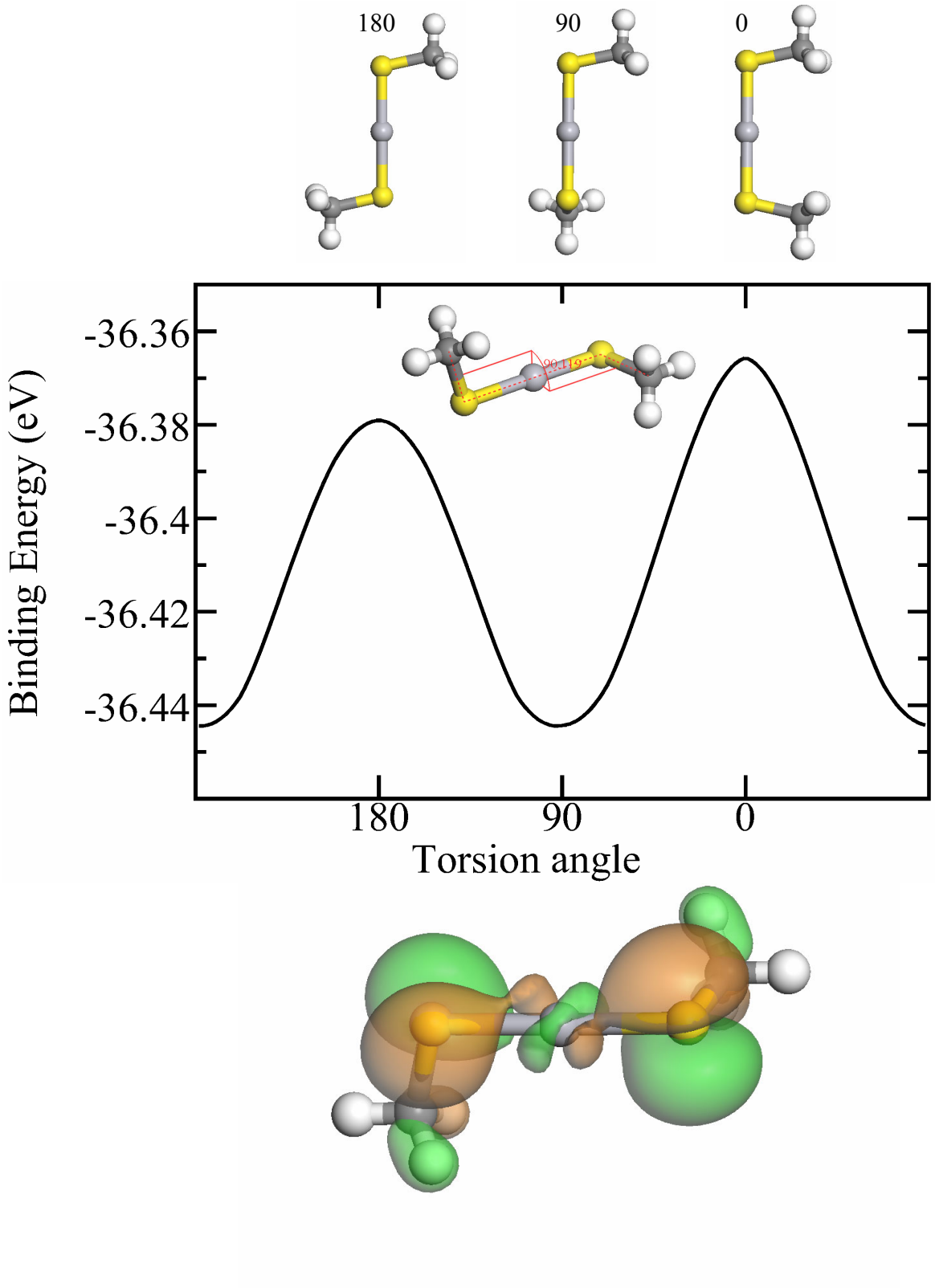
180
90
0
-36.36
-36.38
-36.4
-36.42
-36.44
Binding Energy (eV)
180
90
0
Torsion angle

Figure 8

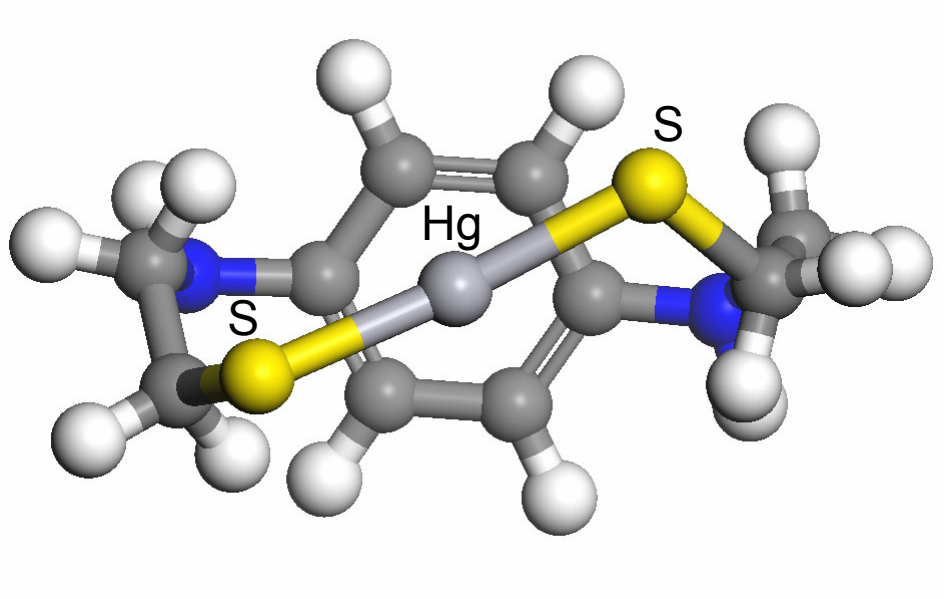

Figure 9